JOURNAL OF GEOPHYSICAL RESEARCH, VOL. 112, D12209, doi:10.1029/2005JD006049, 2007

Nitric acid condensation on ice: 2. Kinetic limitations, a possible "cloud clock" for determining cloud parcel lifetime

B. Gamblin,[1,2] O. B. Toon,[1,3] M. A. Tolbert,[2,4] Y. Kondo,[5] N. Takegawa,[5] H. Irie,[6] M. Koike,[7] P. K. Hudson,[8] J. O. Ballenthin,[9] D. E. Hunton,[9] T. M. Miller,[9] A. A. Viggiano,[9] B. E. Anderson,[10] M. Avery,[10] G. W. Sachse,[10] K. Guenther,[11] C. Sorenson,[11] and M. J. Mahoney[12]

Received 5 April 2005; revised 12 May 2006; accepted 23 August 2006; published 27 June 2007.

[1] Measurements of NO_Y condensation on cirrus particles found in stratospherically influenced air sampled during the SOLVE-I mission are analyzed and compared with data from other field studies of HNO_3 or NO_Y condensation on ice. Each field study exhibits an order of magnitude data spread for constant HNO_3 pressures and temperatures. While others assumed this distribution is due to random error, the data spread exceeds instrument precision errors and instead suggests HNO_3 removal had not attained equilibrium at the time of sampling. During the SOLVE-I mission, condensation on ice was a significant sink for HNO_3 despite submonolayer surface coverages; we therefore propose condensation of HNO_3 on lower-stratospheric cirrus particles is controlled by kinetics and will occur at a kinetically limited rate. Furthermore, we suggest the low accommodation coefficient for HNO_3 on ice combined with relatively short-lived clouds causes highly scattered, limited HNO_3 uptake on cirrus particles. We couple laboratory data on the accommodation coefficient of HNO_3 on ice with field surface coverage data in order to generate a ''cloud clock'': a calculation to determine the age of a cloud parcel. Data from the aforementioned field studies are compared to theoretical models for equilibrium surface coverage on the basis of laboratory data extrapolated to atmospheric temperatures and HNO_3 pressures. This comparison is difficult because most of the atmospheric data are probably not at equilibrium and follow a condensation time curve rather than an equilibrium surface coverage curve. Finally, we develop a simple mathematical solution for the time required for HNO_3 condensation on ice.

Citation: Gamblin, B., et al. (2007), Nitric acid condensation on ice: 2. Kinetic limitations, a possible ''cloud clock'' for determining cloud parcel lifetime, *J. Geophys. Res.*, *112*, D12209, doi:10.1029/2005JD006049.

[1]Laboratory for Atmospheric and Space Physics, University of Colorado, Boulder, Colorado, USA.
[2]Department of Chemistry and Biochemistry, University of Colorado, Boulder, Colorado, USA.
[3]Department of Atmospheric and Oceanic Sciences, University of Colorado, Boulder, Colorado, USA.
[4]Cooperative Institute for Research in Environmental Sciences (CIRES), University of Colorado, Boulder, Colorado, USA.
[5]Research Center for Advanced Science and Technology, University of Tokyo, Tokyo, Japan.
[6]Frontier Research Center for Global Change, Japan Agency for Marine-Earth Science and Technology, Yokohama, Kanagawa, Japan.
[7]Department of Earth and Planetary Physics, University of Tokyo, Tokyo, Japan.
[8]Department of Chemistry, University of Iowa, Iowa City, Iowa, USA.
[9]Air Force Research Laboratory, Hanscom AFB, Massachusetts, USA.
[10]NASA Langley Research Center, Hampton, Virginia, USA.
[11]NASA Dryden Flight Research Center, Edwards, California, USA.
[12]Jet Propulsion Laboratory, California Institute of Technology, Pasadena, California, USA.

0148-0227/07/2005JD006049$09.00

1. Introduction

[2] It has been suggested that condensation on sedimenting cirrus clouds could be a significant loss mechanism for nitric acid in the upper troposphere and lower stratosphere [*Lawrence and Crutzen*, 1998]. HNO_3 condensation on settling ice particles could either permanently remove HNO_3 from the atmosphere or redistribute the HNO_3 to lower, warmer altitudes where the ice particles can evaporate and release nitric acid. Redistributed HNO_3 can then be photolyzed to produce NO_X species, which further react to form tropospheric O_3. Condensation of nitric acid on cirrus clouds could therefore either permanently remove ozone producing species or redistribute the O_3 precursors to other altitudes. Ozone is a greenhouse gas; therefore in order to correctly understand and model the Earth's radiative forcing and climate change potential, it is necessary to correctly understand the concentration and partitioning of HNO_3 near the tropopause.

[3] Many laboratory studies have been conducted to understand the equilibrium surface coverage of HNO_3 on

ice and the accommodation coefficient associated with this process [*Abbatt*, 1997; *Aurora et al.*, 1999; *Zondlo et al.*, 1997; *Aguzzi and Rossi*, 2001; *Hudson et al.*, 2002; *Hynes et al.*, 2002]. The surface coverage in these studies varies significantly as does its functional dependence on nitric acid partial pressure and temperature. Numerous field studies have also attempted to understand condensation of HNO_3 on ice by measuring HNO_3 or NO_Y on cirrus ice particles, but these studies also have widely varying results [*Weinheimer et al.*, 1998; *Meilinger et al.*, 1999; *Kondo et al.*, 2003; *Popp et al.*, 2004; *Ziereis et al.*, 2004]. Additionally, field data often do not agree well with laboratory data and no one laboratory-based model seems to link laboratory and field data in all cases or experimental/field conditions. Most laboratory conditions include nitric acid pressures and temperatures that fall in different regimes than found in the atmosphere. Several groups have used various theories to extend the laboratory data to atmospheric conditions. However, laboratory studies are conducted at equilibrium conditions, and it is an assumption of previous studies that the atmospheric data have reached equilibrium. Here we examine whether this is a good assumption.

[4] Field measurements of HNO_3 or NO_Y on ice particles have varying results. As discussed below, some studies suggest HNO_3 or NO_Y surface coverage depends on temperature, others suggest the process of HNO_3 or NO_Y condensation on ice instead depends on HNO_3 vapor pressure, and there are other studies which do not observe either of these trends. For example, *Weinheimer et al.* [1998] present observations of NO_Y on ice clouds at temperatures from 208–211 K. Their calculations show that all of the gaseous HNO_3 (assumed to be 15% of NO_Y) may have been depleted by condensation on ice in a relatively large surface area wave cloud in under 2 min. By contrast, a study by *Meilinger et al.* [1999] found very little HNO_3 present on a cold ($T \approx 196$ K) ice cloud. *Kondo et al.* [2003] found NO_Y does not condense appreciably on warmer temperature, upper tropospheric cirrus ice clouds ($T > 215$ K), while it does condense on colder clouds ($T < 215$ K). Similarly, *Ziereis et al.* [2004] observed coverages greater than 1 percent of a monolayer for temperatures below 217 K although only 1% of the available gas-phase NO_Y was found in the particulate phase. *Popp et al.* [2004] found 16–100% of the total HNO_3 condensed on cirrus cloud particles. They found that the fraction of total HNO_3 in the condensed phase increased strongly with surface area density. *Kondo et al.* [2003], *Popp et al.* [2004], and *Ziereis et al.* [2004] found HNO_3 (or NO_Y) surface coverage in the atmosphere has a strong dependence on temperature and/or gas-phase NO_Y or HNO_3 abundance.

[5] *Kondo et al.* [2003] and *Gamblin et al.* [2006] have shown that during the SOLVE-I mission, condensation on ice is a significant sink for NO_Y despite submonolayer surface coverages. *Gamblin et al.* [2006] reexamined the SOLVE-I surface coverage data and found that the process of NO_Y condensation on ice behaves differently at different regimes of O_3 abundance. At $[O_3] < 100$ ppbv ("lower altitude" or "upper tropospheric" air), HNO_3 is not the predominant species condensing to form particulate NO_Y but may compete with other NO_Y species when condensing on upper tropospheric ice (N_2O_5 is suggested as the primary component). Conversely, at $[O_3] > 100$ ppbv ("higher altitude" or "lower stratospheric" air), HNO_3 is found to be the primary species condensing on ice. Here we discuss the lower-stratospheric *Kondo et al.* [2003] SOLVE-I data in comparison with other recent field studies. Assuming that at high altitudes, HNO_3 is the predominant component of condensed NO_Y, HNO_3 surface coverage was calculated from the SOLVE-I data set by first subtracting the *Kondo et al.* [2003] gas-phase NO_Y data from their total NO_Y data, to obtain particulate NO_Y. Each particulate NO_Y value was then divided by the corresponding FSSP-300 surface area at that particular time and the NO_Y instrument enhancement factor to obtain a value for surface coverage in units of molecules/cm^2. This calculation is described in further detail by *Gamblin et al.* [2006]. We examine SOLVE-I data, specifically data collected on 23 January 2000, and show that the large spread in the SOLVE-I surface coverage data occurs because, at the time of sampling, HNO_3 condensation on ice had not attained equilibrium. We then show that calculated cloud lifetimes and relatively low accommodation coefficients of "Non-NAT", HNO_3 containing particles, as measured in the laboratory, suggest nitric acid often does not have sufficient time to condense appreciably on lower-stratospheric cirrus cloud particles at the HNO_3 abundances observed. These same ideas are then applied to other field data.

2. Atmospheric Data Comparison

[6] For the SOLVE-I mission, only higher-altitude data (where $[O_3] > 100$ ppbv) from the *Gamblin et al.* [2006] "data set" were examined in this study. As shown by *Gamblin et al.* [2006], at $[O_3] > 100$ ppbv HNO_3 is the primary component of NO_Y that has condensed on ice. Furthermore, the surface area for the $[O_3] > 100$ ppbv SOLVE-I data was increased by a factor of 2, as discussed by *Gamblin et al.* [2006], because the FSSP-300 is known to underrepresent cirrus cloud surface areas [*Heymsfield et al.*, 1990] and studies suggest the instrument could measure surface areas low by a factor of 2 to 10 (*Kondo et al.* [2003], *Hallar et al.* [2004], respectively). Assuming these constraints, Figure 1 is a plot of the *Kondo et al.* [2003] NO_Y surface coverage data as a function of HNO_3 gas pressure in Torr, shown as differently colored "plus" symbols. The SOLVE surface coverages are organized into three different temperature bins, with each temperature bin corresponding in color to the "Field Data" legend on the right side of the plot. The high-altitude SOLVE data we analyzed ranged in temperature from approximately 198 to 206 K and in HNO_3 pressure from approximately 10^{-8} to 10^{-7} Torr. These data suggest that at high altitudes, NO_Y surface coverage is independent of HNO_3 gas pressure.

[7] Also included in Figure 1 are results from the BIBLE (larger, colored, solid circles), INCA (smaller, black, solid circles), POLSTAR-1 (dark blue "x"), and SUCCESS (light blue "x") field studies of NO_Y on cirrus (data from the *Popp et al.* [2004] study are outside the scope of this manuscript). Since these latter data sets are near the tropopause, NO_Y species other than HNO_3 could be condensing (*Gamblin et al.* [2006] suggest N_2O_5 as the primary possibility) but we do not have the information to determine if nitric acid is the only NO_Y constituent condensing on these particles. In that sense the surface coverages may be

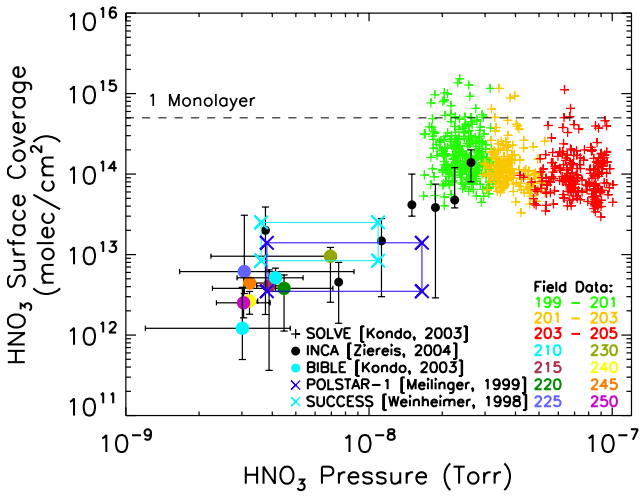

Figure 1. HNO_3 surface coverage (molecules/cm^2) versus HNO_3 gas pressure in Torr. The color of each data point represents different sampling temperatures and corresponds, respectively, to the colored temperature in the field data legend. The SOLVE data are shown as "plus" symbols and include only lower-stratospheric data, where $[O_3] > 100$ ppbv. Surface area of the SOLVE data has been increased by a factor of 2, as discussed by *Gamblin et al.* [2006]. Also included for comparison are results from four field studies of NO_Y condensation on cirrus particles: BIBLE [*Kondo et al.*, 2003], shown as colored circles, and INCA [*Ziereis et al.*, 2004], shown as smaller, black, solid circles. The dark and light blue "x" symbols represent the boundary of possible surface coverages from the POLSTAR-1 [*Meilinger et al.*, 1999] and SUCCESS [*Weinheimer et al.*, 1998] data, respectively. Surface coverage was not specifically calculated in the *Meilinger et al.* [1999] and *Weinheimer et al.* [1998] study; therefore maximum and minimum surface coverages were determined from the range of gas-phase HNO_3 or NO_Y, particulate NO_Y and surface area presented. The temperature of the *Meilinger et al.* [1999] data is approximately 196 K, whereas temperatures from the *Weinheimer et al.* [1998] study cover 208–211 K. The INCA data are averages over nitric acid pressure intervals of 3.75×10^{-9} Torr, restricted to temperatures between 212 and 217 K. The dashed line labeled "1 Monolayer" indicates one monolayer of HNO_3 molecules on ice, 5×10^{14} molecules/cm^2. We used Torr as a unit for nitric acid because it is conventional in laboratory studies. 1 Torr is the same as 1.33 hPa.

upper limits for HNO_3 condensation. However, it is not likely that N_2O_5 would be present at the ambient conditions since the measurements for the BIBLE, INCA, POLSTAR-1 AND SUCCESS missions were taken in the daytime. The colored circles represent observed NO_Y surface coverages for median HNO_3 pressures using data collected over the tropical Pacific Ocean at temperatures of 210–250 K during the BIBLE campaign (August–September 1998 and 1999) [*Kondo et al.*, 2003]. The differently colored data points correspond to the different sampling temperatures as shown in the "Field Data" legend in Figure 1. The black solid circles represent HNO_3 coverages measured between 212–217 K during the INCA campaign [*Ziereis et al.*, 2004], averaged over HNO_3 pressure intervals of 3.75×10^{-9} Torr. The INCA campaign took place in March/April and September/October of 2000, out of Punta Arenas, Chile and Prestwick, Scotland, respectively.

[8] The dark and light blue "x" symbols represent outer bounds of possible surface coverages from the POLSTAR-1 [*Meilinger et al.*, 1999] and SUCCESS [*Weinheimer et al.*, 1998] data, respectively. The temperature of the *Meilinger et al.* [1999] data is approximately 196 K, whereas temperatures from the *Weinheimer et al.* [1998] study cover 208–211 K. Surface coverage was not specifically calculated in the *Meilinger et al.* [1999] and *Weinheimer et al.* [1998] study; therefore maximum and minimum surface coverages were determined from the range of gas-phase HNO_3 or NO_Y, particulate NO_Y and surface area presented in each study.

[9] For each field data set, an order of magnitude data spread can be seen for constant nitric acid pressures and temperatures. Other studies [*Popp et al.*, 2004; *Ziereis et al.*, 2004] have reported similar large data spreads and have assumed it was due to random error. The data have then been treated by averaging a data set over specific temperature and/or pressure intervals. However, the reported precision of the measurements is approximately 10–15%, which is much less than the data spread seen in Figure 1. (Unfortunately the FSSP instrument used in the SOLVE data has a limited particle size range and might miss large particles. We cannot exclude in that data set the variability that is caused by changes in particle surface area that are not observed. However, other data sets, such as that of *Popp et al.* [2004] show the same level of variability but do have particle sizing instruments over the entire size range. There can also be additional factors leading to larger errors in the measurements of NO_Y than 10–15%. For example, the instrument enhancement factor depends on particle size, yet that variability is not included in the use of the enhancement factor. However, it seems unlikely that this source of error can be large enough to explain order of magnitude variations in the measured particulate NO_Y.) Therefore the data spread exceeds instrument error, suggesting at the time of measurement, nitric acid removal had not yet attained equilibrium. Instead of averaging field data of HNO_3 or NO_Y condensation on ice, we suggest the highest data points are most likely to be closer to equilibrium and therefore one must at least analyze the data with respect to the highest surface coverages and even that may be a lower limit.

[10] Nearly all the surface coverage data from all five field studies in Figure 1 are submonolayer, where one monolayer is indicated by the dashed line at 5×10^{14} molecules/cm^2 [*Hudson et al.*, 2002]. In the following sections, we suggest that the submonolayer HNO_3 coverages on cirrus clouds are due to a relatively low accommodation coefficient in combination with a short cloud lifetime such that HNO_3 molecules did not have enough time to reach equilibrium on the cloud before being sampled.

3. Kinetics of HNO_3 Condensation on Ice: Accommodation Coefficient Comparison

[11] Figure 2 compares laboratory studies of the HNO_3 accommodation coefficient as a function of temperature.

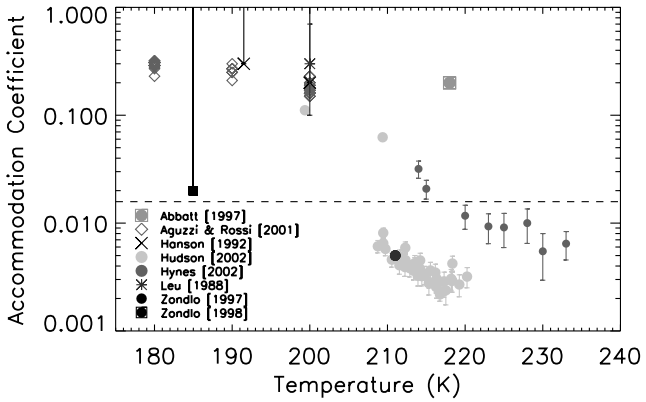

Figure 2. A comparison of laboratory studies of the HNO_3 mass accommodation coefficient on ice as a function of temperature. The dashed line shows the approximate location of a suggested phase change, where data below the line are believed to be of a different phase than data above the dashed line. The *Abbatt* [1997] data point is of the same phase as data below the dashed line.

Some studies spectroscopically identified the phase of the HNO_3-water surface (e.g., a nitric acid hydrate, a supercooled solution or HNO_3 adsorbed on the ice surface), whereas other studies determined which phase should be the most thermodynamically stable at the given temperature and pressures for HNO_3 and H_2O. The dashed line shown in Figure 2 shows the approximate location of the change from limited adsorption to unlimited condensation. Except for the one *Abbatt* [1997] data point, data above the dashed line are assumed to be condensed phase nitric acid, while the data below this line are adsorbed nitric acid.

[12] Figure 3 groups the data from Figure 2 by phase according to our best understanding of the temperature, P_{HNO_3} and P_{H_2O} data presented in each study. Figure 3a shows data where either spectroscopic identification or thermodynamic calculations suggest a supercooled solution (SCS) or any of the nitric acid hydrate (NAH) species ($HNO_3 \cdot nH_2O$, n = 1, 2 or 3) may have existed. Figure 3b represents only data where the phase is suggested to be nitric acid adsorbed to water-ice, called here "Non-NAT".

[13] In studies of the accommodation coefficient, the HNO_3/ice phase of the *Hudson et al.* [2002] data, shown as light gray circles, and the *Zondlo et al.* [1997, 1998] data, shown as black circles and a black circle-square, respectively, were each identified via IR spectroscopy (Figure 3). For some of the data points from the *Hudson et al.* [2002] and *Zondlo et al.* [1997, 1998] studies, calculations suggested either a nitric acid hydrate (NAH) or a supercooled solution (SCS) should be the most thermodynamically stable phase; however, spectroscopic analyses more accurately identified the phase to be "Non-NAT". In these cases, we categorized the data on the basis of spectroscopic studies and did not simply rely on theory alone. It does not appear that the phase of data from the *Abbatt* [1997] (light gray circle-square), *Aguzzi and Rossi* [2001] (gray diamonds), *Hanson* [1992] (black X) and *Hynes et al.* [2002] (dark gray circles) studies were identified spectroscopically. Therefore to determine the most likely phase of these data sets, we compared P_{HNO_3} from their HNO_3 uptake experiments to the calculated NAT saturation vapor pressure and placed their data in the "Non-NAT" regime, Figure 3b, if $P_{HNO_3} < P_{NAT}$ or in the SCS/NAH regime, Figure 3a, if $P_{HNO_3} > P_{NAT}$. The *Leu* [1988] study does not mention phase or nitric acid vapor pressure. A similar comparison of P_{HNO_3} and P_{NAT} at the temperature of this experiment suggests the *Leu* [1988] P_{HNO_3} would have to have been less than 2.7×10^{-8} Torr to avoid formation of NAH or SCS. This value of P_{HNO_3} is significantly lower than any other nitric acid vapor pressure analyzed in our study and therefore it seems reasonable to suggest a nitric acid hydrate or SCS as the most thermodynamically favorable species in this experiment. The light gray circle-square represents the *Abbatt* [1997] study. *Hudson et al.* [2002] questioned whether this data point corresponded with HNO_3 adsorbed on ice or nitric acid dissolved inside a growing ice film.

[14] There is relatively good agreement between the SCS/NAH data. Nitric acid in this regime may have a temperature-dependent mass accommodation coefficient varying from 0.2 at 180 K to 0.02 at 215 K. In the non-NAT data, the agreement between the *Hudson et al.* [2002] and *Hynes et al.* [2002] data is within a factor of 5. The *Abbatt* [1997] point was not included in the comparison because the phase of this data point may be unclear [*Hudson et al.*, 2002]. We conclude from Figures 2 and 3 that the uptake coefficient for HNO_3 adsorption on ice is in the range from about 0.003 to 0.01.

4. Kinetics of HNO_3 Condensation on Ice: Cloud Lifetime

[15] To understand the kinetics of HNO_3 condensation on lower-stratospheric ice particles, we examine the theory of the two different time constants of this process. Case I is the time (T_{gas}) required to deplete the gas-phase nitric acid, essentially examining the process of condensation from the perspective of the gas-phase molecule. Case II is the growth

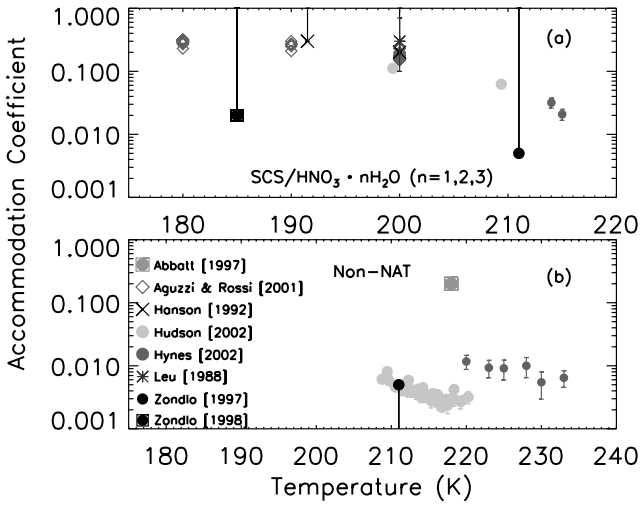

Figure 3. Mass accommodation coefficient versus temperature (K), where the data have been segregated by phase. (a) Data of nitric acid hydrates or supercooled solutions; (b) the "Non-NAT" condensed data.

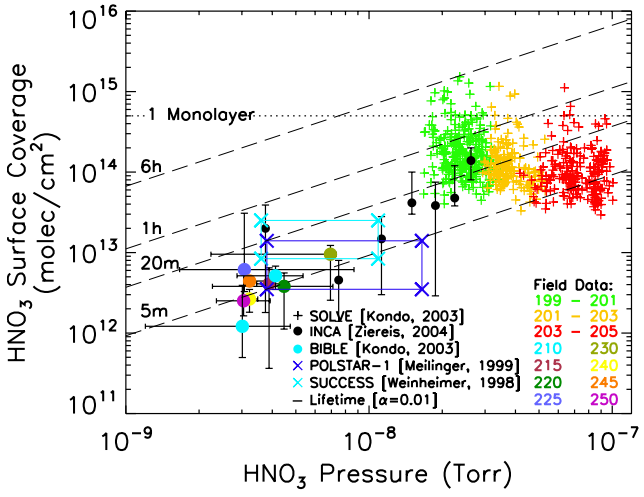

Figure 4. HNO_3 surface coverage (molecules/cm^2) versus HNO_3 gas pressure in Torr, where the surface area of the SOLVE data has been increased by a factor of 2, as discussed by *Gamblin et al.* [2006]. This plot compares the field data shown in Figure 1 with theoretical values of the surface coverage expected by allowing nitric acid to condense for 5 min, 20 min, 1 hour, and 6 hours on an ice particle, assuming an accommodation coefficient of 0.01 (dashed lines), the average temperature (200 K), a range of P_{HNO_3} ($10^{-9} - 10^{-7}$ Torr), and that condensation is not limited by availability of adsorption sites. This calculation essentially examines the minimum time a cloud parcel would have had to exist before being sampled in order to produce the surface coverages in this figure. For example, with 2×10^{-8} Torr of HNO_3 vapor, it would take nearly 6 hours for the uppermost SOLVE data points in green to have obtained their surface coverages, assuming an accommodation coefficient of 0.01. The dotted line labeled "1 Monolayer" indicates one monolayer of HNO_3 molecules on ice, 5×10^{14} molecules/cm^2 [*Hudson et al.*, 2002].

time ($T_{particle}$) for the surface coverage on a particle of a given size with a given amount of condensing gas, which examines the process of condensation from the view of the particle. The details of the calculation of T_{gas} and $T_{particle}$ are given in Appendix A. These times are two different perspectives of viewing one process. Therefore while the equations describing each perspective have different functional dependencies, there is actually only one condensation time and T_{gas} and $T_{particle}$ should produce the same result. In fact, Appendix A shows that the two different cases, T_{gas} and $T_{particle}$ can be mathematically reduced to produce the same equation. Therefore one can discuss the kinetics of HNO_3 condensation in terms of T_C, or the cloud lifetime.

[16] When any gas-phase species, having a sufficiently low mass accommodation coefficient (less than or equal to 0.01 at pressures typical of the upper troposphere/lower stratosphere), condenses on sufficiently small particles (diameter <36 μm), the lifetime of a cloud parcel in which equilibrium has not been reached, T_c can be calculated using kinetic theory from equations (1) and (2).

$$T_s = -\frac{4}{A\bar{c}\alpha} \tag{1}$$

$$T_c = T_s \ln\left(\frac{C_g(f)}{C_g(i)}\right) = T_s \ln\left(\frac{n_g}{n_g + n_p}\right) \tag{2}$$

In equations (1) and (2), A is the surface area density (μm^2/cm^3), $\bar{c}$ is the mean molecular speed (cm/s), α is the mass accommodation coefficient, $C_g(i)$ is the assumed "initial concentration" of the gas-phase species (moles/cm^3), or the sum of the concentration of gas-phase (n_g) and particulate-phase species (n_p). $C_g(f)$ is the "final concentration", or the concentration of the gas-phase species remaining in the air at the time of sampling (after condensation on the particle has occurred). n_p and n_g have units of molecules/cm^3. The full derivation and validation of these equations are discussed in Appendix A.

[17] Examining this idea of cloud lifetimes in reverse, in Figure 4 we assumed cloud lifetimes (the time available for a known amount of gas to condense on a cloud particle before being sampled) of 5 min, 20 min, 1 hour and 6 hours and an accommodation coefficient of 0.01 [*Hynes et al.*, 2002] (Figure 3b) and then determined how much surface coverage one would expect from a given abundance of nitric acid. In this calculation, we assumed a temperature of 200 K and a range of nitric acid pressures encompassing those found in the *Gamblin et al.* [2006] SOLVE "data set" (10^{-9}–10^{-7} Torr). The assumptions made in this calculation are slightly different than those made for T_C and are discussed further in Appendix B. Figure 4 shows the resulting theoretical surface coverage as a function of nitric acid pressure for an accommodation coefficient of 0.01 (dashed lines), assuming four different cloud lifetimes, and compares this data to the field data seen previously in Figure 1. For example, with 2×10^{-8} Torr of HNO_3 vapor, it would take approximately 6 hours for the uppermost SOLVE data points in green to have obtained their surface coverages, assuming an accommodation coefficient of 0.01. This calculation essentially examines how long a cloud parcel would have had to exist before being sampled for the surface coverages shown in Figure 4 to be produced.

[18] The slopes of the cloud lifetimes seen in Figure 4 resemble the slope implied by the data from the five field studies. Therefore this slope in the atmospheric data may have been produced by kinetics limiting the surface coverage. It is suggested that at the time of sampling for a given nitric acid abundance, the data points with smaller surface coverages did not have as much time for nitric acid to condense on the ice particles relative to the sampled particles having higher surface coverages. Perhaps none of these particles had attained equilibrium (we are unable to identify equilibrium for reasons discussed below) by the time of sampling, but they had made varying amounts of progress depending on the lifetime of the cloud parcel, thus explaining the data scatter along the cloud lifetime curves. Because these data sets cover approximately 2 orders of magnitude of nitric acid pressure, this suggests condensation of HNO_3 on ice in the atmosphere is often controlled by kinetics. Back trajectories from SOLVE-I suggest that these lifetimes are reasonable as discussed below.

[19] Back trajectories were used to approximate the history of the air parcels observed on 23 January 2000. Output from the NASA Goddard Space Flight Center (GSFC) Trajectory Model for cloudy regions sampled

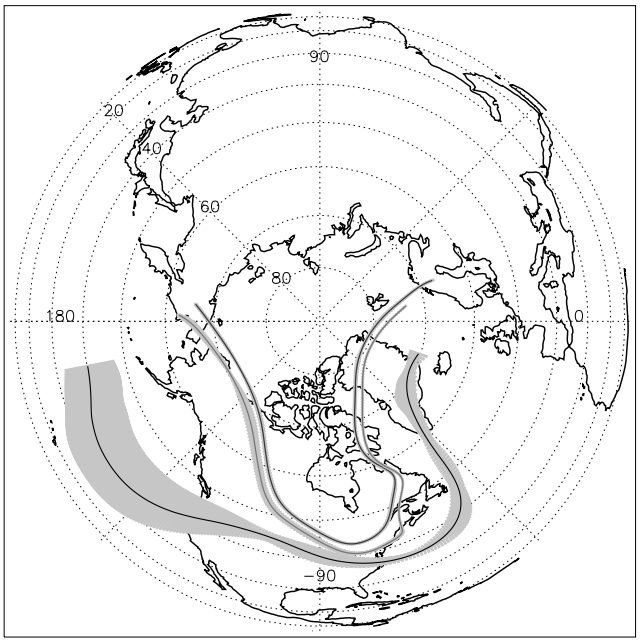

Figure 5. NASA GSFC back trajectories initialized along cloudy flight segments sampled by the DC-8 on 23 January 2000 during the SOLVE-I mission. The three trajectories shown as solid curves represent the mean of three groupings of trajectory paths. The shaded regions represent a 1 standard deviation in the trajectory locations in each group.

during this flight shows the possible path of the clouds before they were sampled between Greenland and Scandinavia (Figure 5). Only the mean of three groups of trajectory paths is shown for clarity. In Figure 5, the solid curves represent the mean trajectory for three different groups of trajectory paths. The shaded region surrounding the solid

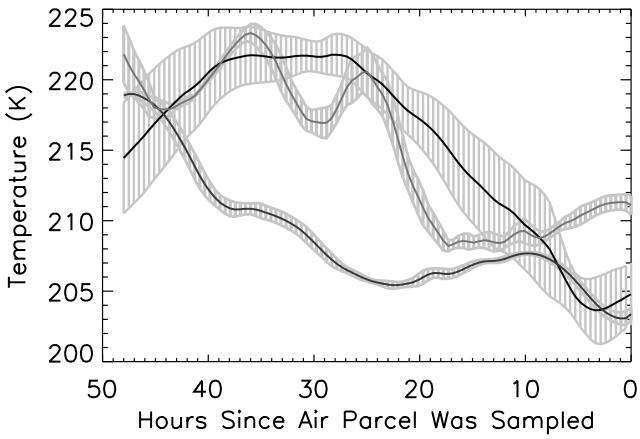

Figure 6. The mean temperature history associated with the three groups of back trajectories shown in Figure 5. When the x-axis is zero, the air mass was sampled by the instruments on board the DC-8 aircraft on 23 January 2000. Air parcel age increases to the left. The three trajectories shown as solid curves represent the mean of three groupings of trajectories. The shaded regions represent a 1 standard deviation in the trajectory temperature history in each group.

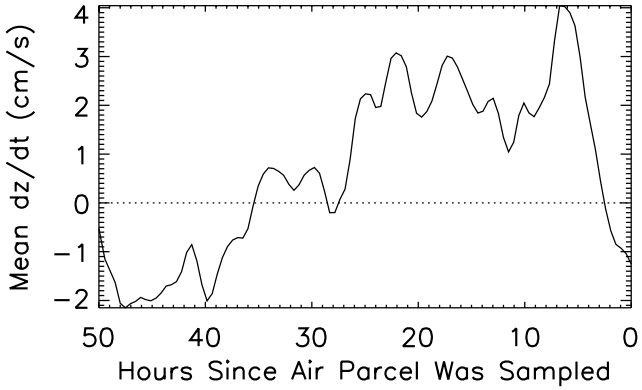

Figure 7. The mean change in altitude with time (dz/dt) of the air parcels shown in Figures 5 and 6, using the NASA GSFC back trajectory analyses.

curve of each group represents the standard deviation of the trajectory locations for that group. Temperature along each of the three mean back trajectories was examined to determine the vertical motion of the air parcels. Figure 6 shows the mean temperature history associated with the three groups of trajectories shown in Figure 5. At zero hours the air mass was sampled by the instruments on board the DC-8 aircraft on 23 January 2000 during the SOLVE-I mission and the air mass age increases to the left. It can be seen that most of the air parcels were cooling and therefore the air was ascending for the previous 2 days before being sampled. This ascent suggests sedimentation had not occurred to a significant degree before the air masses were sampled. To more clearly understand the vertical motion, Figure 7 shows the mean change in altitude with time (dz/dt) of all the air parcels sampled (where only the mean of three groups is shown in Figures 5 and 6). Figure 7 shows that for most of the previous 26 hours before the air parcels were sampled, they experienced strong updrafts up to 4 cm/s. The data shown in Figures 6 and 7, along with typical fall speeds for particles of the size sampled during the SOLVE mission (3–20 μm) of at most 1 cm/s [*Seinfeld and Pandis*, 1998, p. 466] suggest that sedimentation had not occurred to a significant degree for the previous 30 hours before the air masses were sampled. Furthermore, as discussed by *Gamblin et al.* [2006], we assumed any particles sampled at the time of flight generally existed in the cloud near the sampling altitude throughout their lifetime.

[20] To determine an approximate cloud parcel lifetime using the back trajectory analyses, air parcel saturation (S_{ice}) along the three mean back trajectories (Figure 8) was calculated. In performing these calculations, we used the temperature along the back trajectories to compute the vapor pressure and we assumed the total amount of water (vapor mass plus ice mass) represented the original vapor content of the air at the time of condensation. This assumes none of the ice particles had fallen from the cloud before it was sampled. Since the mass of ice present at the time of measurement is on average only 15% of the mass of the vapor, the assumption of how much ice may have fallen out before the air parcel was sampled does not make much difference in the final amount of computed total water and hence does not significantly affect the value of S_{ice}, which

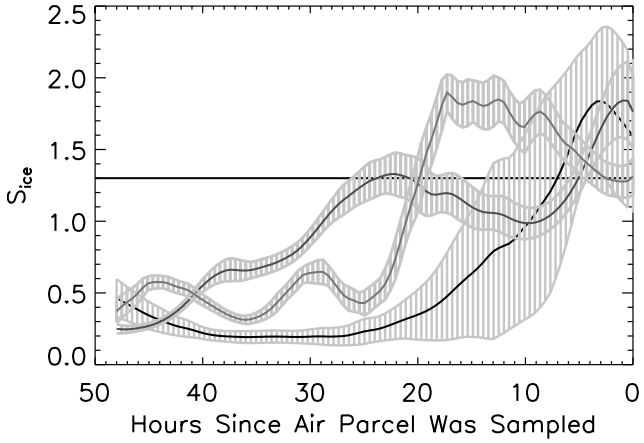

Figure 8. Air parcel supersaturation versus hours before sampling for cloud parcels sampled on 23 January 2000 during the SOLVE-I mission. The horizontal line indicates a supersaturation of 1.3. The suspected cloud origin is where S_{ice} last becomes greater than 1.3 before the air parcel was sampled. This figure assumes no particles have fallen out before the air mass was sampled. As in Figures 5 and 6, the three trajectories shown as solid curves represent the mean of three groupings of trajectories. The shaded regions represent a 1-standard deviation in the trajectory supersaturation in each group.

instead is mainly controlled by the temperature. Furthermore, Figures 6 and 7 suggest it is unlikely that cloud particles observed could have been significantly removed from their respective altitudes over the previous day before measurement.

[21] From left to right on the x-axis of Figure 8, the back trajectory analysis is moving forward in time; at zero, the air parcel was sampled by instruments on board the DC-8. When the supersaturation (S_{ice}) of the air parcels rises above 1.3 (horizontal line) we assume a cloud could have formed. We further assume the cloud that the instruments sampled formed at the last place where the S_{ice} of mean trajectory rises above the 1.3 threshold. According to the back trajectory analysis, most of the air masses reached an S_{ice} of 1.3 approximately 4 to 20 hours before being sampled by the DC-8. One expects much of the cloud mass to have a shorter lifetime than the cloud itself, since atmospheric mixing will evaporate and recondense portions of the cloud as it evolves. As back trajectory analyses are inherently uncertain and because there is uncertainty inherent in estimating cloud lifetimes on the basis of supersaturations calculated from back trajectory data, this supersaturation analysis serves only to demonstrate that our calculation of cloud lifetime from the SOLVE data (Figure 4) is not unreasonable. For example, if the supersaturation-based (back trajectory) cloud lifetimes had been on the order of minutes, this would have suggested the cloud lifetimes shown in Figure 4 were in error.

[22] The lower-stratospheric data seen in Figure 1 were used in Figure 9 to create a histogram of the age of the cloud parcel needed to condense the observed amount of condensed NO_Y (0.5–288 pptv), at the observed amount of HNO_3 gas (26–684 pptv), at the observed temperature (199–206 K), on an ice particle with observed particle sizes from the data (combinations taken from the SOLVE-I "data set" [*Gamblin et al.*, 2006]). Using the data in Figure 3b, we assumed a value of $\alpha = 0.1$ [*Abbatt*, 1997], $\alpha = 0.01$ [*Hynes et al.*, 2002] and $\alpha = 0.005$ [*Hudson et al.*, 2002], represented in Figure 9 by the red, green, and blue histograms, respectively. (Note that we have extrapolated each of these three laboratory-based accommodation coefficient data sets out to temperature and pressure regimes found in the upper troposphere/lower stratosphere.) The blue histogram suggests in the lower stratosphere, using an accommodation coefficient of 0.005, the amount of condensed NO_Y sampled during the SOLVE mission would require nearly a day to condense on the ice particles, while the green histogram, for an accommodation coefficient of 0.01, shows HNO_3 could condense at the observed level in less than 10 hours. Both scenarios are consistent with back trajectory studies of cloud parcel age (Figure 8). Assuming an accommodation coefficient of $\alpha = 0.1$, nitric acid condensing on an ice cloud would require less than 1 hour to condense at the observed levels. Typical cirrus cloud lifetimes are often much longer than minutes. Therefore if

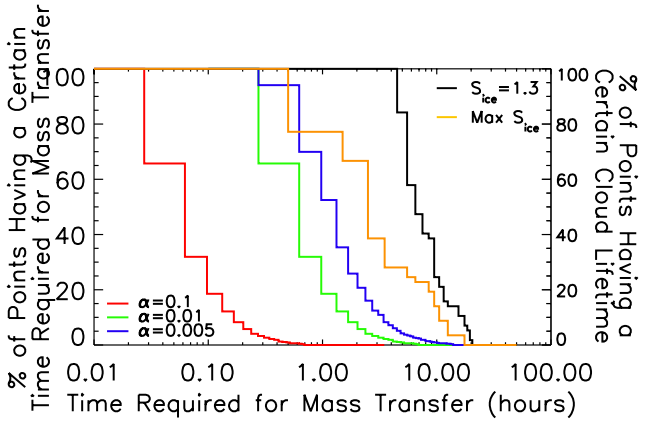

Figure 9. Percent of points in the data set having a certain calculated time required to condense a given amount of HNO_3 at a given temperature onto a particle of given diameter, using three different accommodation coefficients. The red histogram was obtained using an accommodation coefficient, α, of 0.1 [*Abbatt*, 1997], the green histogram assumed an α of 0.01 [*Hynes et al.*, 2002], and the blue histogram was determined using an α of 0.005 [*Hudson et al.*, 2002]. This plot examines only higher-altitude (lower-stratospheric) data, where $[O_3] > 100$ ppbv. The surface area used in the time for mass transfer calculations was increased by a factor of 2 to agree with Figures 1 and 4. The black and yellow histograms refer to the right-hand y-axis. These histograms count the percent of data points from the back trajectory analysis (Figure 8) having a certain cloud lifetime. The black histogram counts the number of points for a certain cloud parcel age where the supersaturation first rises above 1.3 before the air mass was sampled, and the yellow histogram counts the number of points where the maximum supersaturation occurred. When calculating total water to determine the supersaturation, it was assumed that no particles had fallen out from air parcel before it was sampled.

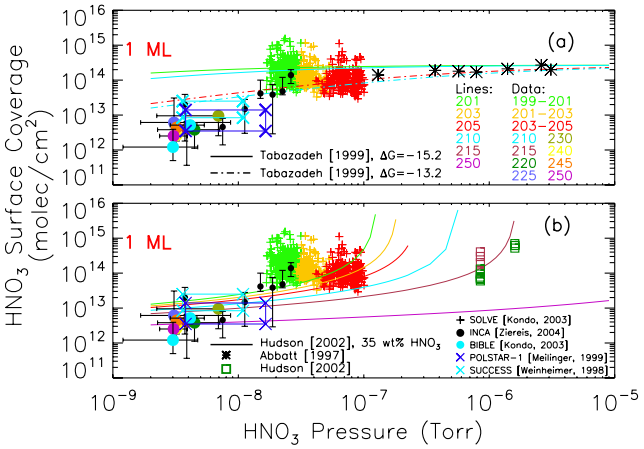

Figure 10. HNO_3 surface coverage (molecules/cm^2) versus HNO_3 gas pressure in Torr, as seen in Figure 1. All legends shown in this figure apply to both (a) and (b). Included in Figure 10a are results of the *Tabazadeh et al.* [1999] modeling study of the *Abbatt* [1997] laboratory data (shown here as black asterisks, where T = 228 K). The *Tabazadeh et al.* [1999] model assumed, for example, a $\Delta G = -15.2$ kcal/mol (dash-triple-dotted lines) and $\Delta G = -13.2$ kcal/mol (dash-dotted lines). The solid lines in Figure 10b represent an extrapolation of the fit to data from the original *Hudson et al.* [2002] laboratory study of HNO_3 on ice surfaces at 35 wt % HNO_3. The *Hudson et al.* [2002] data are shown as squares, where the maroon data represent temperatures between 212 and 215 K and the dark green data represent temperatures between 215 and 220 K.

an accommodation coefficient of 0.1 were reasonable, we would expect much higher surface coverages than those observed. The exact lifetime of the clouds are not known, therefore this value of the accommodation coefficient cannot be completely discounted.

[23] The black and yellow histograms refer to the right-hand y-axis. These histograms examine the number of back trajectory analyses from Figure 8 having a certain cloud lifetime. The black histogram counts the percent of data points along the $S_{ice} = 1.3$ line in Figure 8 having at least the shown cloud parcel age and the yellow histogram counts the percent of data points having at least a certain cloud parcel age from when the maximum supersaturation occurred. For example, as seen by the yellow histogram, over 75% of the back trajectories reached a maximum supersaturation more than 1 hour before the air parcel was sampled. The black histogram suggests that more than 80% of the back trajectories have a cloud lifetime of at least 5 hours.

[24] The *Hynes et al.* [2002] data ($\alpha \approx 0.01$) and the *Hudson et al.* [2002] data ($\alpha = 0.005$) (Figure 3b) seem reasonable for the higher-altitude, lower-stratospheric SOLVE data, as they afford an agreement between the cloud lifetime required for HNO_3 condensation calculations (Figure 4) and back trajectory models of the air parcel (Figure 8). Figure 9 shows that using a larger value of HNO_3 accommodation coefficient to calculate the time required for mass transfer produces a shorter amount of time necessary for the HNO_3 to condense onto an ice particle, but is still consistent with plausible values of cirrus cloud lifetimes.

[25] We conclude that kinetic factors control the uptake of HNO_3 on an ice particle. A positive feature of this process is that if the accommodation coefficient of HNO_3 on ice is known, accurate measurements of cloud particle surface coverages and particle sizes would allow calculation of the ice crystal lifetime, creating a "cloud clock" which measures the age of a cloud parcel. Hopefully between laboratory, aircraft and satellite observations this clock can be used to learn more about cloud lifetimes and to calibrate the clock. For example, many sorts of clouds, such as contrails and cumulus have well defined origins. By measuring the amount of nitric acid on such clouds one can determine what the growth rate and mass accommodation coefficient must have been. Once the accommodation coefficient is known, then the lifetime of other cloud parcels can be determined by the amount of nitric acid on the ice and in the gas phase.

5. Comparison of Equilibrium Nitric Acid Coverages: Atmospheric and Laboratory Measurements

[26] When comparing atmospheric and laboratory data, laboratory based models for equilibrium nitric acid surface coverage on ice need to be extrapolated out of their measurement range to atmospheric conditions, particularly for nitric acid partial pressures. Moreover, the laboratory data disagree not just quantitatively but also qualitatively. Trying to decide between different theoretical models for extrapolating the laboratory data is complicated because much of the atmospheric data have apparently not come to equilibrium and therefore represents the lifetime of the cloud and the condensation rate, rather than the equilibrium surface coverage measured in the laboratory. Figure 10 compares atmospheric nitric acid coverage measurements with laboratory studies of nitric acid surface coverage on ice and models used to fit these laboratory data.

[27] Figure 10a shows the data presented in Figure 1 and includes surface coverages determined from the *Abbatt* [1997] laboratory study (asterisks, T = 228 K) and the *Tabazadeh et al.* [1999] surface chemistry model of HNO_3 scavenging by cirrus cloud particles, designated by the colored dash-dotted lines. *Tabazadeh et al.* [1999] fit the *Abbatt* [1997] data using a Langmuir adsorption isotherm for equilibrium surface coverage, θ, (equation (3)), where α is the fraction of surface sites available for adsorption, K_{eq} is the equilibrium adsorption constant, and P_g is the vapor pressure of the adsorbed gas over the surface (Torr). In equation (4), $C = 1.111 \times 10^6$ (kg$^{1/2}$K$^{1/2}$Torr^{-1}sec^{-1}mol$^{-1/2}$), M is the molecular weight of the adsorbing gas in kg, T is the temperature in K, R is the gas constant and ΔG_{ads} is the free energy of adsorption per mole (kcal/mol).

$$\theta = \frac{\alpha K_{eq}^{1/2} P_g^{1/2}}{1 + K_{eq}^{1/2} P_g^{1/2}} \tag{3}$$

$$K_{eq} = \frac{C}{10^{13}(\mathrm{sec}^{-1})\sqrt{MT}} \exp\left[\frac{\Delta G_{ads}}{RT}\right] \tag{4}$$

[28] *Tabazadeh et al.* [1999] compare HNO_3 coverage as a function of temperature for three different assumptions of adsorption free energy, −15.2, −14.2 and −13.2 kcal/mol. Shown here are results of the *Tabazadeh et al.* [1999] fit to the *Abbatt* [1997] data, using a free energy of −15.2 kcal/mol (dash-triple-dotted lines) and −13.2 kcal/mol (dash-dotted lines). (The two legends shown in Figure 10 apply to both Figures 10a and 10b). At the P_{HNO_3} under consideration in this study, the *Tabazadeh et al.* [1999] model shows a HNO_3 surface coverage relatively independent of nitric acid pressure. This approximates the same trend seen in the high-altitude SOLVE surface coverage data. In order to compare the temperature dependence of the *Tabazadeh et al.* [1999] surface coverage equation to the temperature trend seen in the high-altitude SOLVE surface coverage data, both the green and red curves (−15.2 kcal/mole at 201 K and −13.2 kcal/mol at 205 K, respectively) are paired with results of the calculation using the same free energy, while using a temperature of 210 K (blue curves). The blue dash-triple-dotted line represents the *Tabazadeh et al.* [1999] surface coverage equation using a free energy of −15.2 kcal/mol and a temperature of 210 K, while the blue dash-dotted line represents the same equation using a free energy of −13.2 kcal/mol and a temperature of 210 K. As seen in Figure 10a, it appears the *Tabazadeh et al.* [1999] model does not fit the slope implied by the BIBLE, INCA, SUCCESS or POLSTAR-1 data or the temperature separation of the high-altitude SOLVE data. Initially, it might seem like Figure 10a could imply that a $\Delta G = -15.2$ kcal/mol for the *Tabazadeh et al.* [1999] curve would fit the SOLVE data, while a $\Delta G = -13.2$ kcal/mol would provide the best fit for the remaining data sets. *Popp et al.* [2004] used the *Tabazadeh et al.* [1999] model and a free energy of −11.0 kcal/mol to fit the CRYSTAL-FACE data of HNO_3 on cirrus particles, while *Ziereis et al.* [2004] used a free energy of −14.2 and −13.0 kcal/mol to fit the INCA data. Although one can alter the *Tabazadeh et al.* [1999] equation to fit different data, it is not reasonable to use a different free energy for each data set.

[29] One might instead reason that the data for nitric acid pressures below about $2 - 3 \times 10^{-8}$ Torr have not reached an equilibrium surface coverage by the time of sampling. The cloud lifetime curves shown in Figure 4 provide a reasonable fit to the atmospheric data for nitric acid pressures lower than $2 - 3 \times 10^{-8}$. For instance, a $\Delta G = -15.2$ kcal/mol for the *Tabazadeh et al.* [1999] curve would fit the SOLVE data and one could assume that all the other data at lower nitric acid pressures are simply far from equilibrium.

[30] In Figure 10b, we further compare atmospheric data with previous laboratory studies of nitric acid condensation on ice, by including results of the *Hudson et al.* [2002] laboratory study of the uptake of HNO_3 on thin ice films (colored squares). The symbol color corresponds to the temperatures shown in the "Data" legend in Figure 10a, where the maroon colored squares indicate data collected at temperatures between 212 and 215 K and the dark green squares represent data collected at temperatures between 215 and 220 K. The multilayer Frenkel-Halsey-Hill (FHH) model for surface coverage (equation (5), solid lines) used in the *Hudson et al.* [2002] laboratory study is extrapolated out of the range over which the data were obtained, down to temperatures and HNO_3 pressures measured during the SOLVE-I campaign. In equation (5), θ represents surface coverage and θ_{max} is the maximum coverage of HNO_3 for one monolayer of HNO_3, or 5×10^{14} molecules cm^{-2} [*Hudson et al.*, 2002]. In our study, P denotes a range of HNO_3 pressures from 10^{-9} to 10^{-6} Torr and P° is the vapor pressure of a 35 wt % HNO_3/H_2O solution used in the *Hudson et al.* [2002] study and determined by interpolating data provided by *Jaecker-Voirol et al.* [1990] (equation (6)).

$$\frac{\theta}{\theta_{\max}} = \left(\frac{A}{\ln\left(\frac{P^\circ}{P}\right)}\right)^B \tag{5}$$

$$\log_{10} P^\circ(Torr) = \left(\frac{-3431.4}{T(K)}\right) + 10.184 \tag{6}$$

[31] The colors of the laboratory isotherms correspond to the colors used to represent the field data; therefore each laboratory curve should be compared to the respective colored field data. With 1×10^{-8} Torr of HNO_3 gas present, one would expect just less than 3×10^{13} molecules/cm^2 of HNO_3 to condense on an ice surface at 201 K, on the basis of extrapolations of the *Hudson et al.* [2002] laboratory data. The extrapolated *Hudson et al.* [2002] laboratory data of HNO_3 surface coverage (solid lines) have a strong dependence on HNO_3 gas pressure and temperature. The temperature separation of the *Hudson et al.* [2002] laboratory curves resemble the trends seen in the high-altitude SOLVE data, where for a given surface coverage the temperature of the data warms as nitric acid pressure increases. It can also be seen that the field data have much larger surface coverages than would be predicted from the laboratory data. One would expect the 199–201 K SOLVE data (green +), for example, to lie on or below the green laboratory curve. When comparing the coldest BIBLE data at 210 K (light blue, solid circles) and the warmest BIBLE data at 250 K (magenta circles) to the *Hudson et al.* [2002] laboratory isotherms at the respective temperatures, it can be seen that the atmospheric data do lie below the laboratory curves as expected. Specific temperature information is not possible for the averaged INCA [*Ziereis et al.*, 2004], SUCCESS [*Weinheimer et al.*, 1998] or POLSTAR-1 [*Meilinger et al.*, 1999] data points; therefore only their trend can be compared with the *Hudson et al.* [2002] model. The trend of the INCA, SUCCESS, and POLSTAR-1 data does also closely resemble extrapolations of the *Hudson et al.* [2002] data, while in some instances the data points lie above the *Hudson et al.* [2002] model. Although the SOLVE data do lie above the *Hudson et al.* [2002] isotherms, these extrapolated laboratory isotherms are being used well outside of the regime where the original data were collected and to which the isotherms were fit.

[32] Assuming ambient atmospheric conditions were different than those encountered in the *Hudson et al.* [2002] laboratory study, the ambient weight percent of HNO_3 in water could have varied from the 35 wt% HNO_3 used in the laboratory. The weight percent of HNO_3 in water was altered to discover how this parameter affects the FHH isotherm model and its relation to the atmospheric data sets. It was determined that minor changes in the weight percent used to determine P° in equations (5) and (6) provide a reasonable fit to the temperature trend shown by the higher-

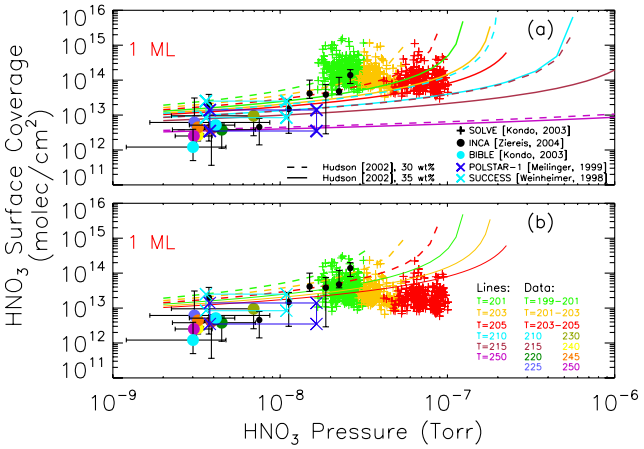

Figure 11. HNO_3 surface coverage (molecules/cm^2) versus HNO_3 gas pressure in Torr, derived from Figure 10b. All legends shown in this figure apply to both (a) and (b). The solid lines in Figure 11a represent an extrapolation of the fit to data from the original *Hudson et al.* [2002] laboratory study at 35 wt % HNO_3. The dashed lines indicate the *Hudson et al.* [2002] isotherms assuming 30 wt% HNO_3. In Figure 11a, the surface area of the lower-stratospheric SOLVE data has been increased by a factor of 2, consistent with all previous figures. The surface area of the lower-stratospheric SOLVE data in Figure 11b has been increased by a factor of 10, as suggested by *Hallar et al.* [2004].

altitude SOLVE data and the slope implied by all three field data sets. This can be seen in Figure 11a, where dashed lines were added to Figure 10b, indicating a HNO_3 in water weight percent of 30%. This represents a decrease of 5% from the original weight percent assumed in the *Hudson et al.* [2002] study.

[33] Alternatively, if the surface area of the high-altitude SOLVE data is increased by a factor of 10, as suggested by *Hallar et al.* [2004], the SOLVE data do lie at or below the *Hudson et al.* [2002] isotherms, regardless of the weight percent assumed. Figure 11b includes dashed lines and solid lines representing extrapolations of the *Hudson et al.* [2002] laboratory data, assuming a HNO_3 weight percent of 30% and 35%, respectively. Either correcting for errors in the measured surface area or correcting for changes in the ambient atmospheric weight percent of HNO_3 in water (or a combination of both methods) allows a reasonable fit of the atmospheric data using extrapolations of data from the *Hudson et al.* [2002] laboratory study. The kinetics of cloud lifetime is necessary to fully explain the distribution of atmospheric data below the *Hudson et al.* [2002] isotherms.

[34] HNO_3 solubility in ice was also examined as a possible cause of the elevated SOLVE surface coverages. We determined that if HNO_3 were simply dissolving in the particles, the particulate NO_Y instrument would detect only very small surface coverages, about an order of magnitude smaller than necessary to explain the elevated surface coverages seen in the HNO_3 field data. Additionally, burial of HNO_3 in a growing ice particle is examined in Appendix C. The results of this analysis suggest burial or particle growth/sublimation does not impact the surface coverage data significantly.

[35] It is difficult to decide between competing models describing atmospheric data, because the atmospheric data may not be at equilibrium. If all clouds had similar lifetimes that were shorter than the equilibration time, then, because of the kinetics of condensation, all the surface coverage data would be closely distributed around the lifetime curves, just as it is in Figure 4.

[36] The *Tabazadeh et al.* [1999] and the *Hudson et al.* [2002] models of HNO_3 condensation on an ice surface have very different dependencies on temperature and nitric acid partial pressure, yet both can fit the available field data given certain assumptions. The kinetics of HNO_3 condensation on ice needs to be better understood before making further comparisons to laboratory data. In addition, further laboratory studies, preferably at atmospheric conditions, are needed to understand the role, if any, that weight percent (atmospheric water vapor) plays in ambient nitric acid surface coverage, determine which model better represents atmospheric data and spectroscopically identify the phase of HNO_3-ice for mass accommodation coefficient studies.

6. Conclusions

[37] It has been shown that field data of HNO_3 or NO_Y condensed on ice have about an order of magnitude data spread for constant P_{HNO_3} and temperature. Since this spread exceeds instrument error, it is suggested that HNO_3 removal from the gas phase had not attained equilibrium at the time of measurement for much of the data collected. Different portions of a cloud may have followed different paths toward equilibrium and had different lifetimes, causing the scattered, submonolayer surface coverages. Calculations suggest that for particles of the sizes encountered during SOLVE, HNO_3 condenses at a kinetically limited rate and that this rate depends on the mass accommodation coefficient. This dependence is useful because accurate surface coverage data and nitric acid gas-phase data coupled with laboratory measurements of the accommodation coefficient can provide a "cloud clock", where the age of a cloud parcel can be determined. For the SOLVE-I data, the lifetime of the clouds observed, on the basis of trajectory studies, is consistent with theoretical predictions of cloud lifetimes needed to explain observed surface coverages. Finally, it is shown that the scatter in surface coverage caused by cloud lifetime makes it difficult to compare laboratory equilibrium coverage data and field data. Both existing theoretical models based on laboratory data can be made to fit the atmospheric data if different assumptions are made. However, kinetics is more likely to explain the trends in the current atmospheric data than are the dependencies on temperature and nitric acid pressure found in the equilibrium surface coverage models. Further laboratory studies would be useful to differentiate between prevailing theories and to better calibrate the "cloud clock".

Appendix A

A1. Time Required to Condense a Gas-Phase Species

[38] To determine the time required to deplete a given amount of nitric acid gas, T_{gas}, we first determined the

change in nitric acid concentration with time (equation (A1)), which incorporates the equation for mass transfer to a single particle, dm/dt, assuming there is no vapor pressure of the condensed species (equations (A2a)–(A2e)) [*Seinfeld and Pandis*, 1998, p. 649]. In equation (A1), C_g is the concentration of nitric acid gas in moles/cm^3, and N(r) is the radius-dependent number density. In the equation for mass transfer (A2a), the correction factor for the diffusion of a species in the transition regime $f(Kn, \alpha)$ (equations (A2b) and (A2c)) was determined using the Fuchs and Sutugin approach [*Fuchs and Sutugin*, 1971; *Seinfeld and Pandis*, 1998, p. 604], where Kn is the Knudsen number, α is the molecular accommodation coefficient, $\bar{c}$ is the mean molecular speed (cm/s) and r is the particle radius (cm). Note we assume here that the surface adsorption sites are not fully occupied so that the accommodation coefficient does not change with time. The Fuchs and Sutugin correction factor [*Seinfeld and Pandis*, 1998, p. 604] is a useful inclusion to the expression of mass transfer because it takes into account the transition between diffusion limited growth and kinetic growth.

$$\frac{dC_g}{dt} = -\int N(r)\frac{dm}{dt}dr \tag{A1}$$

$$\frac{dm}{dt} = 4\pi r f(Kn,\alpha) D_g C_g \tag{A2a}$$

$$f(Kn,\alpha) = \frac{[(0.75\alpha)(1+Kn)]}{[Kn^2 + Kn + (0.283Kn\alpha) + 0.75\alpha]} \tag{A2b}$$

$$Kn = \frac{3D_g}{r\bar{c}} \tag{A2c}$$

$$D_g = 0.559 D_V \tag{A2d}$$

$$D_V = 0.211\left(\frac{T}{T_\circ}\right)^{1.94}\left(\frac{P_\circ}{P}\right) \tag{A2e}$$

$$\frac{dC_g}{dt} = -\int 4\pi r N(r) f(Kn,\alpha) D_g C_g dr \tag{A3}$$

[39] In these calculations, we ignored the simultaneous growth of ice, which we assumed was rapid compared with that of nitric acid (this topic is further examined in Appendix C), and the small dependence of Kn on nitric acid growth. In the above equations, D_g, the diffusion coefficient of HNO_3, was determined using the diffusion equation of water vapor in air (D_V, equation (A2e)) [*Pruppacher and Klett*, 1997] and the equation for gas-phase nitric acid diffusing in air (D_g, equation (A2d)) [*Larsen*, 2000], where T_o is 273.15 K, P_o is 1013.25 mbar, T has units of K, P has units of mbar, and D_V and D_g have units of cm^2/s. When determining the average particle radius, r (cm), we divided the measured particle volume by the particle surface area density for the flight on 23 January 2000 during SOLVE-I.

[40] Full integration of the $f(Kn, \alpha)$ expression in equation (A3) is difficult; therefore for now we will group all radius-dependent terms into the variable δ ($\delta = \int rN(r)f(Kn, \alpha)dr$)and discuss how to treat their integration at the end of this derivation. If we collect the radius-dependent terms and replace them by the variable δ, then equation (A3) reduces to equation (A4).

$$\int_{C_g(i)}^{C_g(f)} \frac{dC_g}{C_g} = -4\pi\delta D_g \int_0^{T_g} dt \tag{A4}$$

[41] In equation (A4), $C_g(i)$ is the assumed ''initial concentration'' of nitric acid before condensation occurred, or the sum of the number of gas-phase (n_g) and particulate-phase HNO_3 (n_p) molecules. $C_g(f)$ is the ''final concentration'' or the gas-phase nitric acid remaining in the air at the time of sampling, after condensation on the particle has occurred. If we set $T_s^{-1} = -4\pi D_g$, then equation (A4) simplifies to that shown in equation (A5).

$$T_g = T_s \ln\left(\frac{C_g(f)}{C_g(i)}\right) = T_s \ln\left(\frac{n_g}{n_g + n_p}\right) \tag{A5}$$

In order to more clearly understand how the concentration of the gas-phase species varies with time (T_g), we rearrange the terms in equation (A5) to produce equation (A6), where the time in question is T_g.

$$C_g(f) = C_g(i) e^{T_g/T_s} \tag{A6}$$

[42] To determine the growth time for the surface coverage on a particle of given size, $T_{particle}$, assuming a given amount of nitric acid gas, we solved the molar flux equation (equation (A7)) [*Seinfeld and Pandis*, 1998, p. 597], where J is the total flow of gas species (moles/s) toward a particle. In equation (A8), the radius-dependent change in surface coverage with time, $d\theta(r)/dt$, is expressed as the molar flux over particle surface area, SA.

$$J = 4\pi r f(Kn,\alpha) D_g C_g \tag{A7}$$

$$\frac{d\theta(r)}{dt} = \frac{J}{SA} = \frac{f(Kn,\alpha) 4\pi r D_g C_g}{4\pi r^2} \tag{A8}$$

Subsequently, in order to determine the change in surface coverage with time over the entire size distribution, $\frac{d\Theta}{dt}$, we must account for the area size distribution as shown in equation (A9).

$$\frac{d\Theta}{dt} = \frac{\int \frac{d\theta(r)}{dt} 4\pi r^2 N(r) dr}{\int 4\pi r^2 N(r) dr} \tag{A9}$$

Again, setting $\delta = \int rN(r)f(Kn, \alpha)dr$, equation (A9) can be simplified as shown below (A10).

$$\frac{d\Theta}{dt} = \frac{4\pi D_g C_g \delta}{\int 4\pi r^2 N(r) dr} \tag{A10}$$

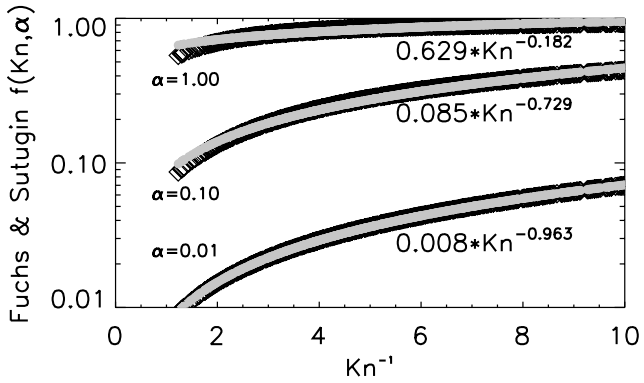

Figure A1. The correction factor for the diffusion of a species in the transition regime, determined using the Fuchs and Sutugin approach [*Fuchs and Sutugin*, 1971; *Seinfeld and Pandis*, 1998, p. 604], assuming three different values of accommodation coefficient, α [0.01, 0.1, 1.0], versus Knudsen number (black). The gray circles represent the least squares fit line to the Fuchs and Sutugin expression, using the form f(Kn, α) = exp(intercept) $\times$ $(Kn^{-1})^{slope}$, where Kn is the Knudsen number.

By integrating the denominator of expression E10 to give the surface area, SA, and by substituting the equation for the time-dependent gas concentration (A6), (A10) reduces to equation (A11) and further to (A12).

$$\int_0^{\Theta} d\Theta = \frac{4\pi D_g \delta C_g(i)}{SA} \int_0^{T_p} e^{\tau/T_s} \tag{A11}$$

$$\Theta = \frac{4\pi D_g \delta C_g(i)}{SA} T_s \left[e^{T_p/T_s} - 1 \right] \tag{A12}$$

Currently the equation to solve for $T_{particle}$ is a function of Θ, which is not a measured quantity; therefore in the final solution for $T_{particle}$ (equation (A13)), we substitute n_p/A for Θ and replace $C_g(i)$ with np + ng, as described above, and then further simplify to produce equation (A13).

$$T_p = T_s \ln\left(\frac{n_g}{n_g + n_p}\right) \tag{A13}$$

Recalling that $T_s^{-1} = -4\pi\delta D_g$ and $\delta = \int rN(r)f(Kn, \alpha)dr$, equation (A13) can be rewritten as equation (A14).

$$T_p = \frac{-1}{4\pi D_g \int rN(r)f(Kn,\alpha)dr} \ln\left(\frac{n_g}{n_g + n_p}\right) \tag{A14}$$

Substituting the $\int rN(r)f(Kn, \alpha)dr$ expression into the δ of the T_s seen in equation (A5) and replacing the contents of T_s, it can be seen that T_g (equation (A5)) is identical to T_p (equation (A14)), as they should be, although they were derived using different equations having different dependencies. Therefore, since T_g is identical to T_p we will begin to develop an expression for T_c, the lifetime of a cloud parcel.

[43] There are several methods of treating the $\int rN(r)f(Kn, \alpha)dr$ term in the denominator of equation (A14). One can simply integrate the size distribution obtained directly from the particle sizing instrument and thereby directly solve for T_C. Alternatively, one can approximate the $f(Kn, \alpha)$ term (A2b) seen in equation (A14) and then complete the integral. Here we discuss an approximation that is valid over all values of mass accommodation coefficient and particle size. (A much simpler approximation, valid only for smaller particles and for mass accommodation coefficients less than or equal to 0.01, is suggested below.) As shown in Figure A1, the full Fuchs and Sutugin equation (in black) (equation (A2b), *Seinfeld and Pandis* [1998, p. 604]) was plotted versus Knudsen number for three accommodation coefficients [α = 1.0, 0.1 and 0.01] using the SOLVE data to determine pressure and temperature. These curves were then fit using the least squares method, where the fit has the form $f(Kn, \alpha) \approx \chi(Kn^{-1})^{slope}$, where χ = exp(intercept). The values of χ and slope are also shown in Figure A1. Making this substitution for $f(Kn, \alpha)$, equation (A14) can be rewritten as shown in equation (A15), where T_C is the lifetime of a cloud parcel.

$$T_C = \frac{-1}{4\pi D_g \chi \int r^{1+slope} N(r)dr} \ln\left(\frac{n_g}{n_g + n_p}\right) \tag{A15}$$

To integrate over radius, we used the solution for the weighted integral of a lognormal size distribution, shown in equation (A16), where β = 1+slope and N_T is the particle number density. The full solution to equation (A15) is then shown in equation (A17) and the terms r_m^{β} and σ will be discussed shortly.

$$\int_0^{\infty} r^{\beta} \frac{dN}{dr} dr = \int_0^{\infty} r^{\beta} N(r)dr = N_T r_m^{\beta} e^{\left(\frac{\beta^2 \ln^2 \sigma}{2}\right)} \tag{A16}$$

$$T_C = \frac{-1}{4\pi D_g \chi N_T r_m^{\beta} e^{\left(\frac{\beta^2 \ln^2 \sigma}{2}\right)}} \ln\left(\frac{n_g}{n_g + n_p}\right) \tag{A17}$$

[44] In equations (A16) and (A17), the terms r_m^{β} and σ are the median diameter and geometric standard deviation of the size distribution, respectively. These parameters of the distribution can be calculated using the definitions of surface area density (A) and volume density (V) (which are reported in the SOLVE data set), equations (A18) and (A19), respectively [*Seinfeld and Pandis*, 1998, p. 414–415], and the solution to the integral shown in equation (A16).

$$A = \int_0^{\infty} 4\pi r^2 N(r)dr = 4\pi N_T r_m^2 e^{\left(\frac{4 \ln^2 \sigma}{2}\right)} \tag{A18}$$

$$V = \int_0^{\infty} \frac{4}{3}\pi r^3 N(r)dr = \frac{4}{3}\pi N_T r_m^3 e^{\left(\frac{9 \ln^2 \sigma}{2}\right)} \tag{A19}$$

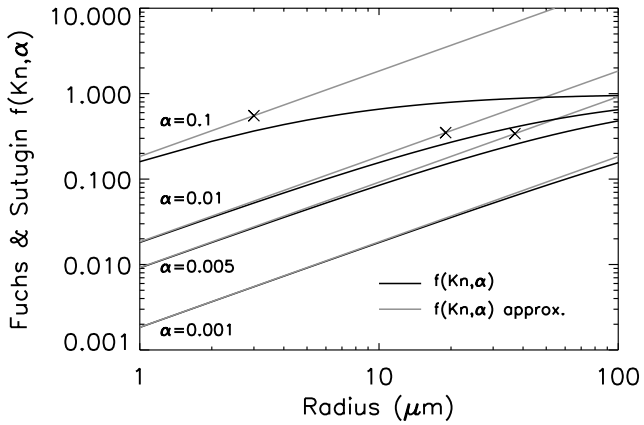

Figure A2. The Fuchs and Sutugin [*Fuchs and Sutugin*, 1971; *Seinfeld and Pandis*, 1998, p. 604] correction factor for the diffusion of a species in the transition regime, assuming four different values of accommodation coefficient [0.001, 0.005, 0.01, 0.1] versus radius in μm (black curves). The light gray curves represent an approximation to the Fuchs and Sutugin expression, using the form f(Kn, α) = 0.75α/Kn. This approximation is only valid for $\alpha \leq 0.01$ and for sufficiently small particles ($D_p \leq 36$ μm). The "X" symbols show the radius at which the f(Kn, α) approximation differs by more than 25% from the Fuchs and Sutugin equation.

The subsequent solution to σ and r_m are shown in equations (A20) and (A21), respectively.

$$\sigma = \frac{(3V)^{1/3}(4\pi N_T)^{1/6}}{A^{1/2}} \tag{A20}$$

$$r_m = \frac{A^{1/2}}{(4\pi N_T)^{1/2}} \cdot e^{\ln^2}\sigma \tag{A21}$$

This solution to T_C is valid for any gas and for any accommodation coefficient, assuming the accommodation coefficient is independent of surface coverage, and assuming there is no vapor pressure of the adsorbed material.

A2. Time Required to Condense a Gas-Phase Species, Assuming $\alpha \leq 0.01$, $D_p \leq 36$ μm

[45] For mass accommodation values at or below α = 0.01 and for particles with sufficiently small diameters, the Fuchs and Sutugin correction factor, $f(Kn, \alpha)$, can be approximated using equation (A22), which is the large Knudsen number (or small particle) limit. Making this substitution into equation (A14) will simplify the process of calculating the lifetime of a cloud parcel for cases where $\alpha \leq 0.01$, because for example, it does not require the calculation or measurement of σ and r_m.

$$f(Kn, \alpha) \Rightarrow \frac{0.75\alpha}{Kn} = \frac{0.75\alpha r\bar{c}}{3D_g} \tag{A22}$$

[46] Figure A2 is a plot of the full $f(Kn, \alpha)$ equation, in black, versus radius for various accommodation coefficients [α = 0.001, 0.005, 0.01 and 0.1]. The approximation to the Fuchs and Sutugin expression (equation (A22)) is shown in gray. This plot shows the $f(Kn, \alpha)$ approximation agrees very well with the original Fuchs and Sutugin approach [*Seinfeld and Pandis*, 1998, p. 604] for low values of accommodation coefficient ($\alpha \leq 0.01$) and particle size, but it does not provide a good fit for larger accommodation coefficients or particles with larger diameter. For example, assuming an accommodation coefficient of 0.1, the approximation does not provide a good fit for any value of radius. The "X" symbols show the radius at which the $f(Kn, \alpha)$ approximation differs by more than 25% from the original Fuch and Sutugin expression [*Seinfeld and Pandis*, 1998, p. 604]. For an accommodation coefficient of 0.01, the $f(Kn, \alpha)$ approximation falls within 25% of the data up to a radius of 18 μm. Assuming an accommodation coefficient of 0.005 and 0.001, the $f(Kn, \alpha)$ approximation is within 25% of the Fuchs and Sutugin equation up to a radius of 36 μm and 200 μm (not shown), respectively.

[47] Substituting equation (A22) into equation (A14), we obtain equation (A23), a more readily solvable form of the equation for the cloud parcel lifetime.

$$T_C = \frac{-1}{\frac{\bar{c}\alpha}{4}\int 4\pi r^2 N(r)dr} \ln\left(\frac{n_g}{n_g + n_p}\right) \tag{A23}$$

The solution to the integral shown in equation (A23) is A, the surface area density (equation (A18)), and the final solution to equation (A23) is T_C' (equations (A24) and (A25)).

$$T_S'^{-1} = \frac{-A\bar{c}\alpha}{4} \tag{A24}$$

$$T_C' = T_S' \ln\left(\frac{n_g}{n_g + n_p}\right) \tag{A25}$$

This equation to calculate the cloud parcel lifetime T_C' is valid only for mass accommodation coefficients less than or equal to 0.01 and for sufficiently small particles ($D_p \leq 36$ μm). If the accommodation coefficient or particle size are greater than the respective values shown, the full equation for T_C (equation (A17)) must be used, because the least squares exponential power fit is required to correctly approximate the $f(Kn, \alpha)$ term.

Appendix B

[48] To derive the equation used to calculate the "time lines" shown in Figure 4 (the theoretical time required to condense the observed surface coverage, assuming a given amount of nitric acid gas at a given temperature and a given mass accommodation coefficient) it must be assumed that the gas concentration does not vary with time, since in this case we do not know the cloud surface areas and hence we do not know the total amount of nitric acid which has condensed. Only the mean surface coverage is known. In this case, we again begin with equation (A8) and then incorporate the $f(Kn, \alpha)$ approximation (equation (A22))

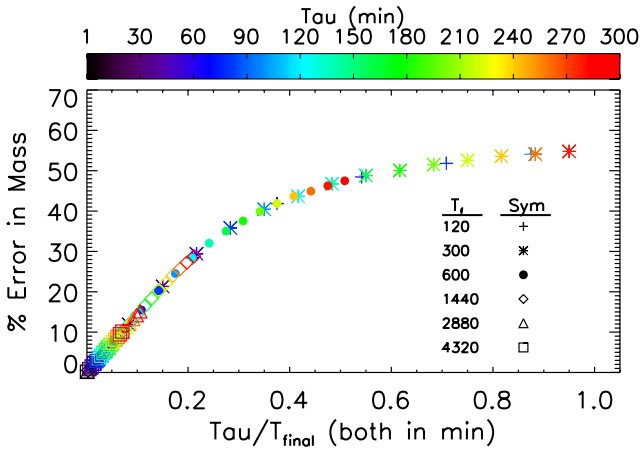

Figure C1. The ratio of the supersaturation e-folding time, Tau, over T_{final} (the total cloud lifetime) versus the percent error in mass condensed assuming the ice particle radius remained constant over the lifetime of the cloud parcel relative to the assumption that the same ice particle grew over time.

into the expression. After canceling variables, equation (A8) reduces to equation (B1).

$$\frac{d\theta}{dt} = \frac{C_g \alpha \bar{c}}{4} \tag{B1}$$

This equation can then be integrated, producing the equation used to calculate the time required to condense the observed nitric acid onto ice particles, equation (B2).

$$T_\theta = \frac{4\theta}{C_g \alpha \bar{c}} \tag{B2}$$

To compare surface coverages for given nitric acid pressures, we assumed fixed times of 5 min, 20 min, 1 hour and 6 hours, a mass accommodation coefficient of $\alpha = 0.01$ and a typical temperature of 200 K. The expected surface coverage versus pressure for an assumed cloud lifetime is shown as dashed lines in Figure 4.

Appendix C

[49] To determine whether the amount of HNO_3 deposited on a growing ice particle differs significantly from the amount deposited on an ice particle in equilibrium, we simulated HNO_3 condensing on an ice particle over a given cloud lifetime (equation (A2a)) and determined the amount of mass that would condense assuming either (1) a radius that remains constant over time, at 10 μm for example, or (2) a radius that increases with time up to 10 μm (equation (C1)).

$$r = \frac{r_{final}\left(1 - e^{-t/\tau}\right)}{\left(1 - e^{-Tf/\tau}\right)} \tag{C1}$$

In the above equation, r_{final} is the maximum size to which a test particle might grow. In our simulation, r_{final} was set to 10 μm, which is an average maximum particle size for the SOLVE-I data set. τ is the supersaturation relaxation time, or the e-folding time for reduction of ice supersaturation due to growing ice crystals [*Jensen et al.*, 2005], T_f is the assumed lifetime of the ice particle from initial nucleation to the time it would be sampled and t is the time evolved since particle growth began.

[50] *Jensen et al.* [2005] suggests that for ice clouds having "surface areas greater than 50 $\mu m^2/cm^3$, the relaxation time is less than about 40 min." As seen in Figure 17 of *Jensen et al.* [2005], there is an inverse relationship between surface area and the supersaturation e-folding time, τ. To encompass typical cirrus cloud lifetimes and the cloud surface areas and relaxation times (τ) seen in the *Jensen et al.* [2005] study, we varied τ and T_{final} (in equation (C1)) from 5–300 min and 2–72 hours, respectively. Further examining the effect of substituting the new equation for radius (equation (C1)) into the radius term of equation (A2a), it can be seen that at t = 0 the radius term (equation (C1)) collapses to zero and as expected, the result of equation (A2a) is that no mass has yet to condense to form an ice particle. Conversely, at $t = T_f$, the radius term reduces to r_{final} and the ice crystal has grown to the final size. It is at this point that we compare how much mass is deposited over the time assuming a growing ice particle and a particle where $r = r_{final}$ throughout all time steps. The latter case was assumed in Appendices A and B.

[51] Figure C1 shows a plot of the relaxation time, τ, over T_{final} (both in minutes) versus the percent error in mass condensed assuming the ice particle radius remained constant over the lifetime of the cloud parcel relative to the assumption that the same ice particle grew over time. The differently colored points represent different combinations of τ and T_{final}. It can be seen from Figure C1 that all possible combinations of the assumed values of τ and T_{final} collapse to form one curve relating the τ/T_{final} ratio to percent error in mass if an ice particle in equilibrium is assumed. Additionally, it can be seen from Figure C1 that the percent error in mass does not ever get much larger than a factor of 2. By correlation, this further suggests the results of the calculation to determine the cloud lifetime assuming a static ice particle (equations (A17) or (A25)) can only have a maximum error near a factor of 2.

[52] **Acknowledgments.** Work performed at the Jet Propulsion Laboratory, California Institute of Technology, was carried out under a contract with the National Aeronautics and Space Administration (NASA). B. Gamblin and Owen B. Toon were supported by NASA.

References

Abbatt, J. P. D. (1997), Interaction of HNO_3 with water-ice surfaces at temperatures of the free troposphere, *Geophys. Res. Lett.*, *24*, 1479–1482.

Aguzzi, A., and M. J. Rossi (2001), The kinetics of the uptake of HNO_3 on ice, solid H_2SO_4-H_2O and solid ternary solutions of H_2SO_4-H_2O-HNO_3 in the temperature range 180 to 211 K, *Phys. Chem. Chem. Phys.*, *3*, 3707–3716.

Aurora, O. P., D. J. Cziczo, A. M. Morgan, and J. P. D. Abbatt (1999), Uptake of nitric acid by sub-micron-sized particles, *Geophys. Res. Lett.*, *26*, 3621–3624.

Fuchs, N. A., and A. G. Sutugin (1971), *Topics in Current Aerosol Research* (*Part 2*), pp. 1–200, Elsevier, New York.

Gamblin, B., et al. (2006), Nitric acid condensation on ice: 1. Non-HNO_3 constituent of NO_Y condensing on upper tropospheric cirrus particles, *J. Geophys. Res.*, *111*, D24210, doi:10.1029/2006JD008266.

Hallar, A. G., L. M. Avallone, R. L. Herman, B. E. Anderson, and A. J. Heymsfield (2004), Measurements of ice water content in tropopause region Arctic cirrus during the SAGE III Ozone Loss and Validation Experiment (SOLVE), *J. Geophys. Res.*, *109*, D17203, doi:10.1029/2003JD004348.

Hanson, D. R. (1992), The uptake of HNO_3 onto ice, NAT and frozen sulphuric acid, *Geophys. Res. Lett.*, *19*, 2063–2066.

Heymsfield, A. J., K. M. Miller, and J. D. Spinhirne (1990), The 27–28 October 1986 FIRE IFO cirrus case study: Cloud microstructure, *Mon. Weather Rev.*, *118*, 2313–2328.

Hudson, P. K., J. H. Schilling, M. A. Tolbert, and O. B. Toon (2002), Uptake of nitric acid on ice at tropospheric temperatures: Implications for cirrus clouds, *J. Phys. Chem. A.*, *106*, 9874–9882.

Hynes, R. G., M. A. Fernandez, and R. A. Cox (2002), Uptake of HNO_3 on water-ice and coadsorption of HNO_3 and HCl in the temperature range 210–235 K, *J. Geophys. Res.*, *107*(D24), 4797, doi:10.1029/2001JD001557.

Jaecker-Voirol, A., J. L. Ponche, and P. Mirabel (1990), Vapor pressures in the ternary system water-nitric acid-sulfuric acid at low temperatures, *J. Geophys. Res.*, *95*, 11,857–11,863.

Jensen, E., L. Pfister, T. Bui, A. Weinheimer, E. Weinstock, J. Smith, J. Pittman, D. Baumgardner, P. Lawson, and M. J. McGill (2005), Formation of a tropopause cirrus layer observed over Florida during CRYSTAL-FACE, *J. Geophys. Res.*, *110*, D03208, doi:10.1029/2004JD004671.

Kondo, Y., et al. (2003), Uptake of reactive nitrogen on cirrus cloud particles in the upper troposphere and lowermost stratosphere, *Geophys. Res. Lett.*, *30*(4), 1154, doi:10.1029/2002GL016539.

Larsen, N. (2000), Polar stratospheric clouds, microphysical and optical models, *DMI Sci. Rep. 00-06*, Danish Meteorol. Inst., Copenhagen.

Lawrence, M. G., and P. J. Crutzen (1998), The impact of cloud particle gravitational settling on soluble trace gas distributions, *Tellus, Ser. B*, *50*, 263–289.

Leu, M.-T. (1988), Laboratory studies of sticking coefficients and heterogeneous reactions important in the Antarctic stratosphere, *Geophys. Res. Lett.*, *15*, 17–20.

Meilinger, S. K., et al. (1999), HNO_3 partitioning in cirrus clouds, *Geophys. Res. Lett.*, *26*, 2207–2210.

Popp, P. J., et al. (2004), Nitric acid uptake on subtropical cirrus cloud particles, *J. Geophys. Res.*, *109*, D06302, doi:10.1029/2003JD004255.

Pruppacher, H. R., and J. D. Klett (1997), *Microphysics of Clouds and Precipitation*, Springer, New York.

Seinfeld, J. H., and S. N. Pandis (1998), *Atmospheric Chemistry and Physics From Air Pollution to Climate Change*, John Wiley, Hoboken, N. J.

Tabazadeh, A., O. B. Toon, and E. J. Jensen (1999), A surface chemistry model for nonreactive trace gas adsorption on ice: Implications for nitric acid scavenging by cirrus, *Geophys. Res. Lett.*, *26*, 2211–2214.

Weinheimer, A. J., T. L. Campos, J. G. Walega, F. E. Grahek, B. A. Ridley, D. Baumgardner, C. H. Twohy, B. Gandrud, and E. J. Jensen (1998), Uptake of NO_Y on wave-cloud ice particles, *Geophys. Res. Lett.*, *25*, 1725–1728.

Ziereis, H., et al. (2004), Uptake of reactive nitrogen on cirrus cloud particles during INCA, *Geophys. Res. Lett.*, *31*, L05115, doi:10.1029/2003GL018794.

Zondlo, M. A., S. B. Barone, and M. A. Tolbert (1997), Uptake of HNO_3 on ice under upper tropospheric conditions, *Geophys. Res. Lett.*, *24*, 1391–1394.

Zondlo, M. A., S. B. Barone, and M. A. Tolbert (1998), Condensed-Phase Products in Heterogeneous Reactions: N_2O_5, $ClONO_2$, HNO_3 Reacting on Ice Films at 185 K, *J. Phys. Chem. A*, *102*, 5736–5748.

B. E. Anderson, M. Avery, and G. W. Sachse, NASA Langley Research Center, Hampton, VA 23665, USA.

J. O. Ballenthin, D. E. Hunton, T. M. Miller, and A. A. Viggiano, Air Force Research Laboratory, Hanscom AFB, MA 01731, USA.

B. Gamblin and O. B. Toon, Laboratory for Atmospheric and Space Physics, University of Colorado, Boulder, CO 80309, USA. (bgamblin@airsci.com)

K. Guenther and C. Sorenson, NASA Dryden Flight Research Center, Edwards, CA 93523, USA.

P. K. Hudson, Department of Chemistry, University of Iowa, Iowa City, IA 52242, USA.

H. Irie, Frontier Research Center for Global Change, Japan Agency for Marine-Earth Science and Technology, 3173-25 Showa-machi, Kanasawa-ku, Yokohama, Kanagawa 236-0001, Japan.

M. Koike, Department of Earth and Planetary Science, University of Tokyo, 7-3-1 Hongo Bunkyo-ku, Tokyo 113-0033, Japan.

Y. Kondo and N. Takegawa, Research Center for Advanced Science and Technology, University of Tokyo, 4-6-1 Komaba Meguro-ku, Tokyo 153-8904, Japan.

M. J. Mahoney, Jet Propulsion Laboratory, California Institute of Technology, Pasadena, CA 91109, USA.

M. A. Tolbert, Department of Chemistry and Biochemistry, University of Colorado, Boulder, CO 80309, USA.